Available online at www.sciencedirect.com
SCIENCE DIRECT®
Journal of Power Sources 137 (2004) 163–174
JOURNAL OF POWER SOURCES
www.elsevier.com/locate/jpowsour

Study of $LiFeO_2$ coated NiO as cathodes for MCFC by electrochemical impedance spectroscopy

Bo Huang [a,*], Qing-chun Yu [b], Hui-min Wang [a], Gang Chen [a], Ke-ao Hu [a,b]

[a] *State Key Laboratory of Metal Matrix Composites, Shanghai Jiaotong University, Shanghai 200030, PR China*
[b] *Institute of Fuel Cell, Shanghai Jiaotong University, Shanghai 200030, PR China*

Received 26 November 2003; received in revised form 1 March 2004; accepted 3 May 2004
Available online13 September 2004

Abstract

$LiFeO_2$ was coated on porous NiO cathode using a simple combustion process. X-ray diffraction (XRD) and scanning electron microscopy (SEM) were employed in the cathode characterizations. The electrochemical behaviors of $LiFeO_2$ coated NiO cathode (LFO-NiO) were also evaluated in a molten 62 mol% Li_2CO_3 + 38 mol% K_2CO_3 eutectic at 650 °C under the standard cathode gas condition by electrochemical impedance spectroscopy (EIS). The impedance response of the NiO and LFO-NiO at different immersion time is characterized by the presence of depressed semicircles in the high frequency range changing over into the lines with the angle of which observed with the real axis differing 45° or 90° in the low frequency range. The experimental Nyquist plots can be well analyzed theoretically with a modified model based on the well known Randles–Ershler equivalent circuit model. In the new model, the double layer capacity (C_d) is replaced by the parallel combination of C_d and b/ω to take into consideration the non-uniform of electric field at the electrode/electrolyte interface owing to the roughness of electrode surface. The LFO-NiO showed a lower dissolution and a good catalytic efficiency close to the state-of-the-art NiO value. In the unit cell test, the performance of the cell composed of $LiFeO_2$ coated NiO cathode maintained more stable values than that of the cell composed of NiO cathode. Thus the cathode prepared with coating method to coat $LiFeO_2$ on the surface of NiO cathode is able to reduce the solubility of NiO to lengthen the lifetime of MCFC while maintaining the advantages of NiO cathode.

Keywords: Molten carbonate fuel cell; Cathode; Solubility; Nickel oxide; Coating; EIS

1. Introduction

The molten carbonate fuel cell (MCFC) is believed to be one of the most promising energy conversion devices that convert chemical energy in fossil fuels into electricity in the near future owing to the high energy conversion efficiency, the excellent environmental characteristics and the ability to utilize a wide variety of fuels such as hydrogen, natural gas and coal gasified gas. However, several hurdles remain before commercialization of MCFC can be realized. The state-of-the-art MCFC nickel cathode, oxidized in situ and lithiated ($Li_xNi_{1-x}O$), presents a relatively high solubility in the electrolyte which can be Li_2CO_3-/K_2CO_3, Li_2CO_3-/Na_2CO_3 or related alkali molten carbonate eutectics. This dissolution leads to the formation of Ni^{2+}, which can diffuse from the cathode toward the anode under a concentration gradient. The dissolved Ni^{2+} precipitates in the sections of matrix, where it encounters dissolved H_2 proceeding from the anode side and is reduced to Ni at a certain distance away from the cathode. The continuous diffusion of Ni^{2+} accelerates more dissolution of nickel from the cathode. Continued deposition of sufficient bridged grains of metallic nickel across the cell eventually causes a short-circuiting of the cell [1,2]. The NiO dissolution also results in loss of active material and a decrease of the active surface area available for the oxygen reduction reaction resulting in degradation of fuel cell performance and durability.

Many efforts have been made to solve the NiO dissolution problem [3–7] and several possible approaches have been studied. More basic molten carbonate melts such as Li/Na carbonate eutectic have been used to decrease the Ni dissolution rate in the melt. Alkaline earth metal salts based on Ba or Sr have also been used as additives to increase the basicity of the melt. However, using more basic molten carbonate melts only partially solves the problem, since these melts decrease the NiO dissolution rate by 10–15% only. In addition, several materials like $LiFeO_2$, $LiCoO_2$, Li_2MnO_3 and $La_{1-x}Sr_xCoO_3$ were also investigated as re-

* Corresponding author. Tel.: +86 21 62933751; fax: +86 21 62822012.
E-mail address: huangbo2k@hotmail.com (B. Huang).

0378-7753/$ – see front matter © 2004 Elsevier B.V. All rights reserved.
doi:10.1016/j.jpowsour.2004.05.015

placement materials for the nickel oxide cathodes because of their extremely low solubility in the carbonate melts [8]. However, the exchange current density for the oxygen reduction reaction on $LiFeO_2$, Li_2MnO_3 and $La_{1-x}Sr_xCoO_3$ is about two to four orders of magnitude lower than that on NiO. Thus, the slow kinetics of the oxygen reduction reaction limits further improvement of cathodes based on these materials. $LiCoO_2$ is more stable than NiO in alkaline environment and is once considered as the most promising alternative cathode material. However, application of $LiCoO_2$ as a cathode material is still limited for producing large area electrodes beyond 1000 cm^2 because of its brittleness and higher manufacturing cost and less electronic conductivity than the conventional NiO cathode. Therefore, these oxides might be inadequate for the cathode material. Recently, new candidate materials such as $LiCoO_2$ or $La_{0.8}Sr_{0.2}CoO_3$ coated NiO cathodes have been proposed [9,10].

In our previous study, a novel NiO cathode was prepared by coating $LiFeO_2$ grains on porous NiO cathode using an auto-ignited combustion process with a citrate-metal nitrate precursor [11]. The present paper is aimed to study the electrochemical behavior of the new cathode material in molten carbonates. The study has been conducted using electrochemical impedance spectroscopy (EIS). The phases and microstructures of the cathode materials before and after immersion in molten carbonate were analyzed by X-ray diffraction (XRD) and scanning electron microscopy (SEM), respectively. The dissolution of the new cathode material in molten carbonates was evaluated using melt analysis.

2. Experimental

2.1. Tape casting

Porous nickel cathodes were prepared by a tape casting and subsequent sintering process. The material system used in this work was based on carbonyl nickel powder, solvent, dispersant, binder and plasticizer. The carbonyl nickel particles (purity: 98%; Shanghai Jinjiang Metal Powder Ltd., China) have a perfect orbicular shape and a narrow size distribution of 2.2–2.8 μm. The solvent system used in this paper consisted of azeotropic mixture of cyclohexanone and butyl alcohol in order to avoid differential evaporation. Glycerol trioleate as a kind of zwitterionic dispersant was used as dispersant. Poly-vinyl-butyl (PVB) and polyethylene glycol (PEG 200) were used as binder and plasticizer, respectively. The PVB binder was supplied as a free flowing fine-grained powder and the PEG plasticizer was obtained in a liquid form. All the organic additives were supplied by Shanghai Chem. Ltd., China. The slurries for the tape casting process were fabricated by a ball milling method that included two steps [12]. In the first step, 50 g of nickel power were added to 1 g dispersant. The ingredients were mixed thoroughly with 40 g cyclohexanone/butyl alcohol solvents and the slurry was ball milled for 4 h in order to break weak agglomerates. Secondly, 5 g PVB and 5 g PEG were added to the above system and the resulting slurry was ball milled for an additional 4 h. After the mixing and the homogenization of the slurry were completed, the slurry was degassed using a vacuum pump (pressure: 200 mbar absolute) and cast on a casting surface of polyethylene film by a “doctor-blade” method. The cast tapes were allowed to dry at room temperature for 48 h. After the solvent in the tapes was completely evaporated, the nickel green tapes were obtained.

2.2. Sintering

Sintering temperature of the tape casted electrodes influences the cathode pore structure and thereby affects its electrochemical performance. Thermogravimetric analysis (TGA) was done to determine the optimum heat treatment schedule for sintering. A typical TGA curve for nickel green tape is shown in Fig. 1. The cast nickel tape was pre-heated at 150 °C for 12 h in order to remove all the solvent in the tape. TGA analysis was done by heating the sample from 100 to 650 °C at a rate of 10 °C/min. A steep reduction in weight was seen on heating the sample at 218 °C due to the removal of the plasticizer. Another two weight losses were noticed between 267 and 400 °C due to the gradual removal of the bind. The removal of all volatile and decomposable organic matter was completed below 400 °C. On heating the sample above 400 °C, oxidation of nickel particle surface took place. Therefore, it is critical to heat the sample in a reducing atmosphere to prevent oxidation during sintering. Further, the rate of heating should be very slow initially to ensure complete burn out of binder and plasticizer. Based on the above TGA, the following heating sequence was used for sintering the porous cathodes: (1) the green tapes were initially heated from room temperature to 200 °C at a rate of 1 °C/min; (2) in the second step, the temperature was held at 200 °C for 2 h; (3) thirdly, the temperature was raised to 400 °C at a rate of 1 °C/min; (4) the temperature was held at 400 °C for 4 h; (5) the temperature was raised to 500 °C at a rate of 2 °C/min; (6) the temperature was held at 500 °C for 2 h; (7) the temperature was raised to 850 °C at a rate of 2 °C/min; (8) the temperature was held at 850 °C for 6 h; (9) in the last step, the samples was cooled to room temperature at a cooling rate of 1 °C/min. Sintering of the green tapes was completed in the 75 vol.% H_2/25 vol.% N_2 atmosphere and the air, respectively.

2.3. $LiFeO_2$ coating

$LiFeO_2$ precursor gel was prepared as follows. Firstly, a stoichiometric lithium nitrate ($LiNO_3$) and iron nitrate ($Fe(NO_3)_3{\cdot}9H_2O$) with a ratio of Li:Fe = 1:1 were dissolved in distilled water, then a stoichiometric amount of citric acid ($C_6H_8O_7{\cdot}H_2O$),which is a chelating agent and fuel, was also

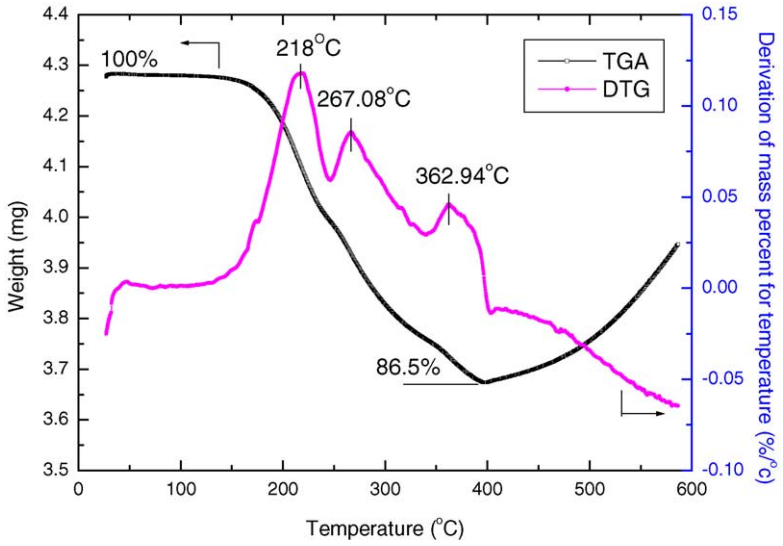

Fig. 1. The TGA/DTG curves of green nickel tape obtained by non-aqueous tape casting.

dissolved in this solution. The stoichiometric ratio of citric acid to nitrates was calculated according to Jain et al. [13]. The Li^+ concentration in the transparent solution was 0.05 mol/dm^3. The sintered porous nickel sheets were dipped in the above solution and evacuated using a vacuum pump set to an absolute pressure of 200 mbar for 30 min so that the solution filled the pores of the nickel sheets. Then the nickel sheets were kept at 450 °C for several minutes and heat-treated at 850 °C for 6 h. This procedure was repeated several times to have a uniform coating. The flow chart for the coating is given in Fig. 2.

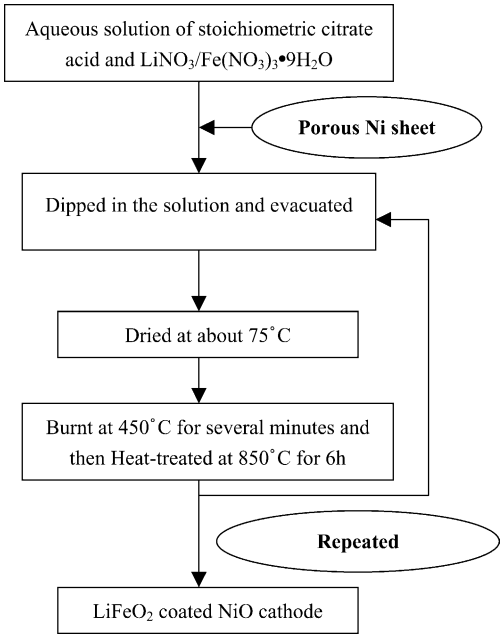

Fig. 2. Flow chart for the preparation process of $LiFeO_2$ coated NiO cathode.

2.4. Electrochemical characterization

The electrochemical characterization of the cathode materials was performed on the porous electrode/molten carbonates interface by means of EIS. The test cell was an alumina crucible contained in a covered quartz vessel. The cover of vessel had been adapted to accommodate a thermocouple, a gas inlet/outlet and two electrodes. The working electrode was composed of the cathode material connected to a Pt lead (0.5 mm in diameter) that is shielded from the electrolyte by an alumina tube sealed by ceramic cement at the base of the tube. The counter electrode was identical to the working electrode. Such a configuration allows elimination of the influence of the counter electrode and avoids the use of a reference electrode that is, by itself, a source of noise [14,15]. Digital mass flow controllers/meters were used to provide the desired gas mixture composition of CO_2 and O_2. The gas mixture was flowed into the melt through a long alumina tube.

The crucible was charged with 300 g eutectic carbonate mixture (62 mol% Li_2CO_3–38 mol% K_2CO_3) and heated to 650 °C in a electric furnace. The eutectic mixture of alkali carbonate, 62 mol% Li_2CO_3–38 mol% K_2CO_3, was made up from AR grade anhydrous reagents (Shanghai Chem. Ltd., China) that had been dried in a furnace at 150 °C. The mixture was purified by a sequence of the following treatments: vacuum drying at 350 °C, fusion/pumping treatment at 700 °C and bubbling of pure CO_2 with the view of neutralizing any O^{2-} formed and decomposing any OH^- ion present. This purification procedure was basically similar to that proposed by Appleby and Nicholson. Gases were of high purity grade and were additionally treated with molecular sieves 5 A and anhydrous $Mg(ClO_4)_2$ to remove traces of water [16,17].

Then the electrodes (Φ 2.4 cm × 0.08 mm) cut out from sintered NiO and $LiFeO_2$ coated NiO (LFO-NiO) were

inserted in the carbonate melt and the cell temperature was kept at 650 °C. The EIS measurements were started 2 h after immersion in the melt in order to obtain a sufficiently stabilized system necessary for an ac-impedance experiment. Various measurements were made from 0 to 100 h under a 0.67 atm CO_2–0.33 atm O_2 gas mixture. The impedance spectra were recorded with a frequency response analyzer Solartron 1260. A 5-mV perturbation amplitude was applied with a frequency scanning range of 10 mHz to 100 kHz at five points per frequency decade.

2.5. Structural characterization and chemical analysis

The structure of the cathode samples sintered at 850 °C in the air for 6 h before and after the electrochemical tests was characterized by scanning electron microscopy (SEM, PHLIPS 515) and X-ray diffraction (XRD, D/max-3A, Cu Kα) at the scanning speed of 4°/min. Porosimetry (Micromeritic 9220) was used to measure the pore size distribution of various cathodes. The porosity and densities of various cathodes were measured by Archimedes' principle in distilled water. In order to determine the structure of the samples after immersion in the molten carbonate, they should be first dissolved in 50 vol.% acetic acid/50 vol.% anhydride mixture aimed to removing the carbonates at the samples surface. Solubility was determined by removing a 0.5 g of molten carbonate from the melts at the appointed time using an alumina rod. Solubility measurements were repeated until their value became concentration that was regarded as the equilibrium solubility. Inductively coupled plasma spectroscopy was carried out to analyze the metal ions equilibrium solubility in the molten carbonate after 200 h of continuous exposure to the molten carbonate.

Table 1
Porosity and bulk density of various cathodes

Porous cathode	Ni cathode	NiO cathode	$LiFeO_2$ coated NiO cathode
Porosity (%)	81.08	75.96	66.12
Density (g/cm^3)	2.09	2.19	2.48

3. Results and discussion

3.1. Microstructural characterization

3.1.1. Cathode characterization

The pore size distributions of the Ni and LFO-NiO cathodes are given in Fig. 3.The average pore diameter of the pure nickel cathode was about 12 μm. After being coated with $LiFeO_2$ and calcined in the air at 850 °C for 6 h, the nickel was oxidized and the average pore diameter decreased to about 8 μm. Table 1 shows textural characterization of the cathodes prepared. It could be seen that the nickel cathode had the largest porosity and lowest density. After being oxidized in the air at 850 °C for 6 h, its porosity decreased from 81.08 to 75.96% and the density increased from 2.09 to 2.19 g/cm^3 due to the sintering effect. In comparison with the Ni cathode, the LFO-NiO had a lowest porosity (66.12%) and a largest density (2.48 g/cm^3), which was duo not only to the sintering effect but also to the coating of $LiFeO_2$ on the porous cathode. It is well known that a cathode with high performance should be of proper porosity (60–80 vol.%) and pore size distribution (6–10 μm), so that the best balance between the solid, liquid and gas phases is maintained during the MCFC operation. Evidently, the LFO-NiO cathode prepared was sufficient to satisfy all requirements of the MCFC operation.

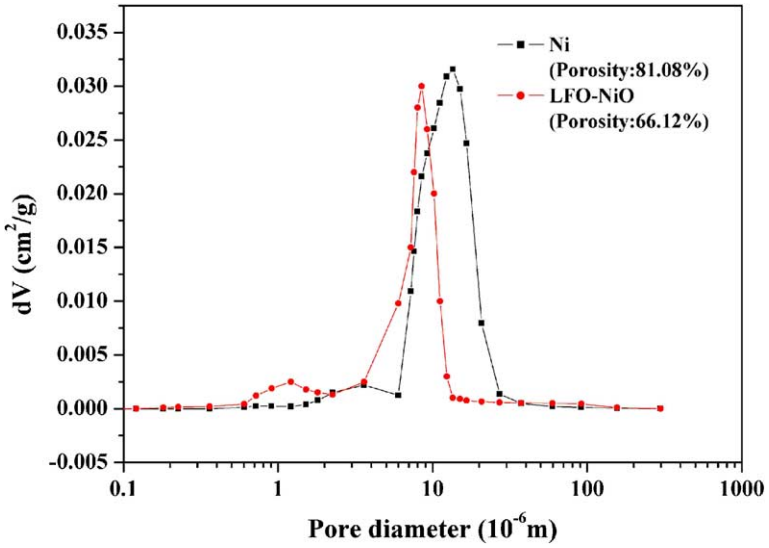

Fig. 3. Pore distribution curves of Ni cathode and LFO-NiO cathode.

3.1.2. SEM characterization

Fig. 4 shows the cross-section SEM micrographs of Ni, NiO and LFO-NiO cathodes, respectively. The morphological difference between Ni and LFO-NiO cathode could be attributed to the $LiFeO_2$ coating on nickel particles surfaces followed by sintering, the particles of LFO-NiO cathode tended to agglomerate together. The $LiFeO_2$ coated NiO cathode had a good pore structure. In comparison with nickel and nickel oxide particles, the surfaces of the pre-treated NiO particles were covered with many tiny grains, which were tightly sintered with the NiO particles. Some small holes were also observed on the $LiFeO_2$ coating due to the release of gases, such as H_2O, CO_2 and N_2, during the combustion procedure of the citrate–nitrate solution in the pores.

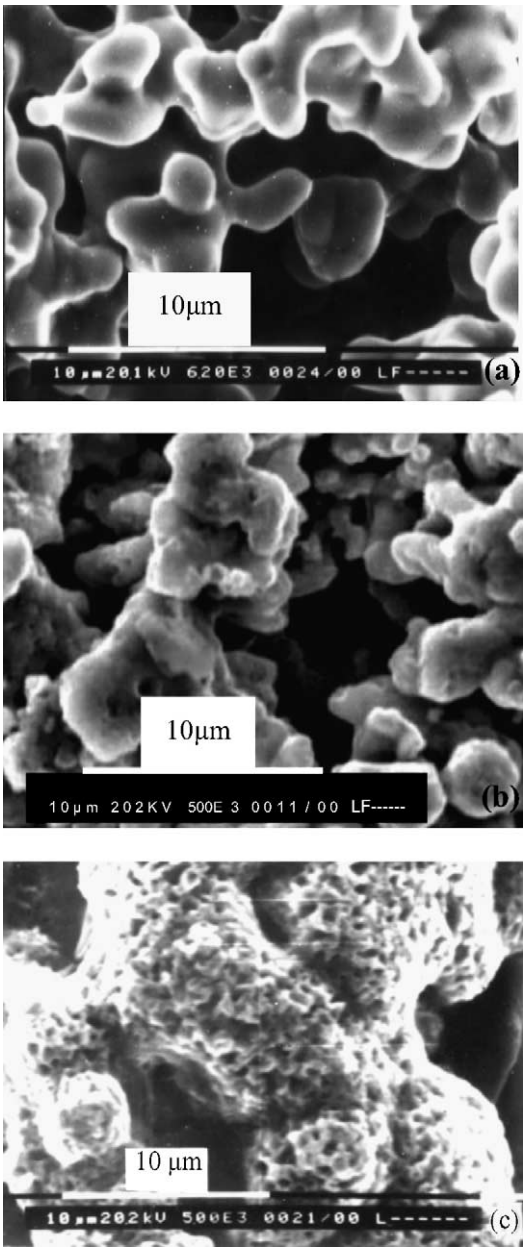

Fig. 4. SEM cross-section micrographs of (a) Ni cathode; (b) NiO cathode; (c) LFO-NiO cathode.

Fig. 5 shows scanning electron micrographs of pure NiO and LFO-NiO cathodes studied before and after the exposure in molten carbonate during 200 h under the standard cathode gas condition (CO_2:O_2, 67:33%). After the electrochemical testing, the pure NiO cathode surface showed marked morphological changes due to the lithiation and dissolution of the material in the molten carbonates. By comparison, no significant differences in the particle size and the surface morphology of $LiFeO_2$ coated NiO cathode were observed before and after immersion in molten carbonate for 200 h.

3.1.3. XRD characterization

Fig. 6 shows the X-ray diffraction patterns of $LiFeO_2$ powders obtained from the gel after heat treatment in different temperatures ranging between 650 and 850 °C. The X-ray diffraction pattern for the gel presents no diffraction peaks, which indicates an amorphous phase. It is clearly seen that the compound formation starts only at 650 °C and crystalline product could be obtained at 850 °C. The X-ray diffraction patterns of LFO-NiO cathode are shown in Fig. 7. The XRD peaks of NiO that appear at 37.24, 43.08, 62.74, 75.28 and 79.28° (2θ) could be observed in the pattern of the NiO cathode. It can also be seen from Fig. 7 that only one peak of $LiFeO_2$ appears at 35.76° (2θ), while other peaks of $LiFeO_2$ that should appear at 37.38, 43.48, 63.22, 75.84 and 79.86° (2θ) are nearly overlapped with the peaks of NiO.

3.2. Solubility test

The dissolution curves of NiO and LFO-NiO cathodes in a molten 62 mol% Li_2CO_3 + 38 mol% K_2CO_3 eutectic is given in Fig. 8. The experimental conditions were kept at 650 °C under a 0.67 atm CO_2/0.33 atm O_2 atmosphere. The dissolution of NiO and LFO-NiO increased significantly with time before 100 h and almost kept constant after 100 h. The NiO cathode had a solubility of 34.3 mol ppm (Ni^{2+}) in the $(Li_{0.62}K_{0.38})_2CO_3$ melts after 200 h, which is similar to the results reported by Motohira et al. [18]. In contrast, the solubility of the LFO-NiO cathode was only 13.5 mol ppm (Ni^{2+}).

The results of solubility tests show that the coating of $LiFeO_2$ on the surface of NiO can significantly retard the dissolution of NiO in molten carbonates. It should be noted that the coating on the surface of the NiO particles consisted mainly of ultrafine $LiFeO_2$ grains, but not a complete $LiFeO_2$ film. Although the $LiFeO_2$ grains were tightly sintered with the NiO particles due to the high instantaneous temperature during the combustion procedure [13], the released gases such as H_2O, N_2 and CO_2 gave rise to holes in the coating, as is shown in Fig. 4c, which means that the coating only reduces the contacting area of the NiO particles with the melts, but does not completely separate the NiO particles from the melts.

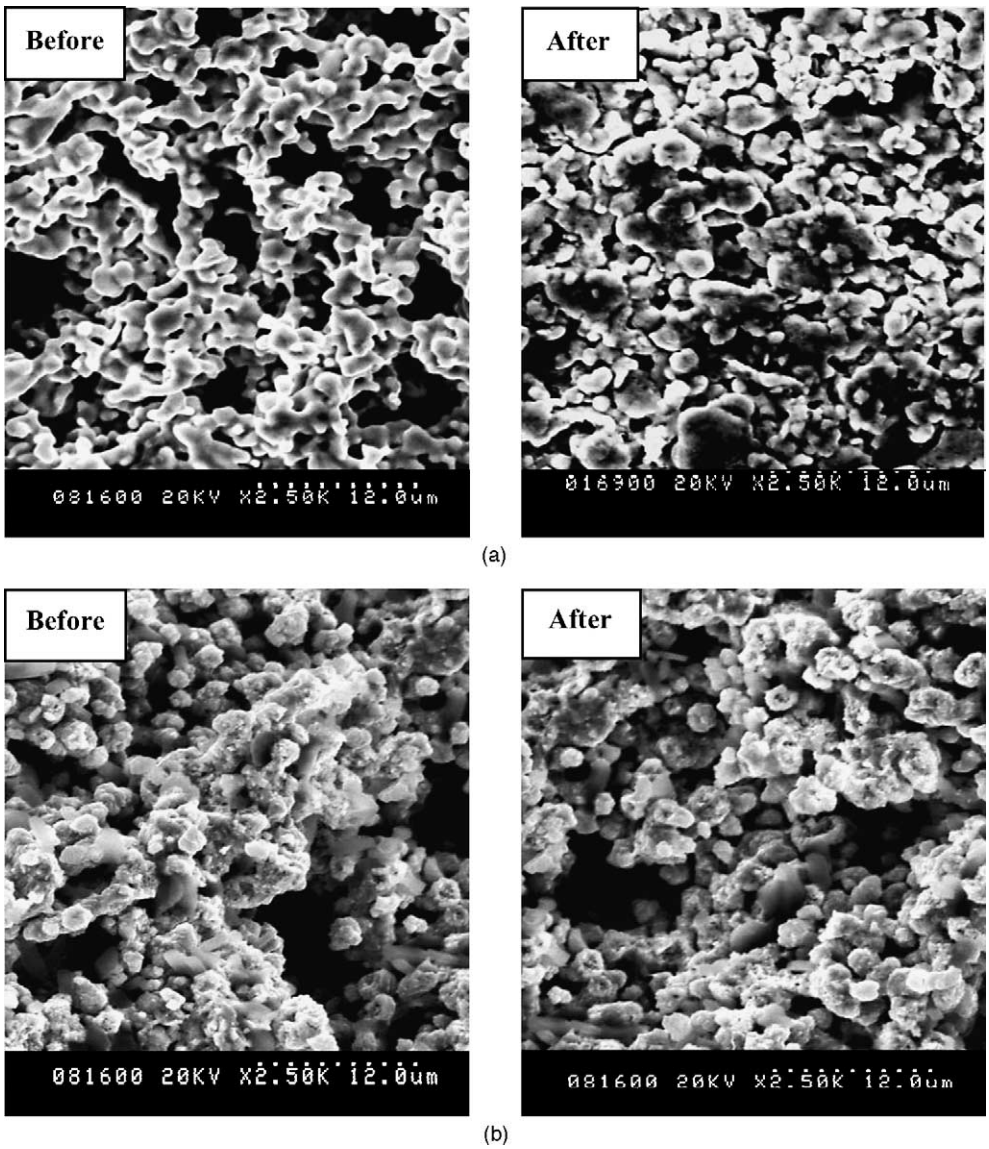

Fig. 5. SEM micrographs corresponding to the two cathode samples before and after testing: (a) pure NiO cathode; (b) LFO-NiO cathode.

The aim of coating the NiO cathode with $LiFeO_2$ is to prolong the time to short circuit of the MCFC. However, a coating with tiny holes cannot completely prevent the dissolution of the inner NiO and the content of nickel ions in the melts will eventually reach the value of that for pure NiO, but the time for this to occur is dramatically extended. This indicates that the dissolution rate (mol ppm h^{-1}) of LFO-/NiO is lower than that of pure NiO. So we infer that the MCFC using LFO-NiO as the cathode has a longer life than that using conventional NiO as the cathode.

3.3. Electrochemical impedance spectroscopy (EIS) study

Fig. 9 depicts the electrochemical impedance spectra for the two cathode materials in a eutectic 62 mol% Li_2CO_3 + 38 mol% K_2CO_3 at 650 °C under a 0.67 atm CO_2/0.33 atm O_2 gas mixture at different immersion time. As it can be seen from the corresponding Nyquist plots, the impedance response of the two cathode materials at different immersion time is characterized by the presence of depressed semicircles in the high frequency range changing over into the lines inclined at varied angles to the real axis in the low frequency range, indicating that the charge transfer resistance (R_{ct}) was dominant. The high frequency plot has been associated with the charge transfer process. In the case of the line at low frequency, it can be concluded that it does not correspond to a mass transfer phenomenon because the angle of the line observed at low frequency with the real axis differs 45° or 90°. It is thought that this line does not correspond to a reaction of the oxygen reduction mechanism. It could correspond to a reaction of a metallic part of the electrode with the melt when the insulating ceramic becomes a little porous. At high frequencies, the plot converged to a value on the abscissa (real

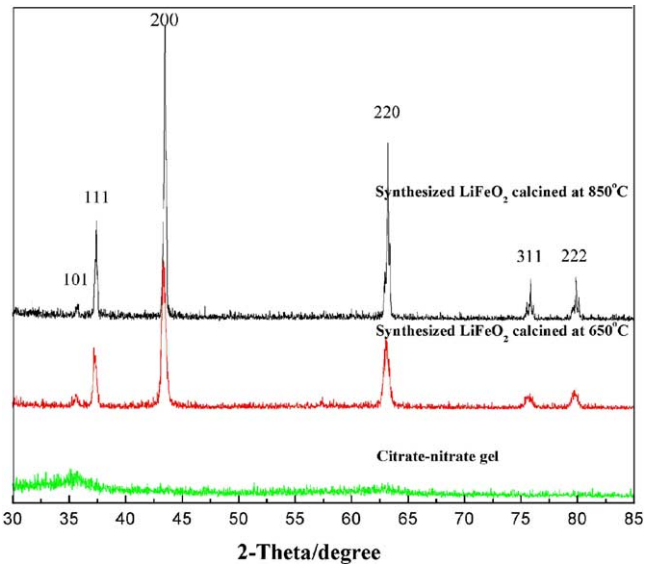

Fig. 6. XRD patterns of citrate–nitrate gel and combustion-synthesized $LiFeO_2$ powder.

axis) as shown in Fig. 9, giving the electrolytic resistance, R_Ω.

For the oxygen reduction reaction on the two cathode materials in Li/K eutectic melts at different immersion time, the empirical plots of impedance on the complex plane were arcs, but their center did not lie on the real axis, as seen in Fig. 9. They may be looked upon as semicircles rotated in the clockwise sense around the origin by a certain angle, θ, as seen in Fig. 10. For the graphic complex plane analysis, the well known Randles–Ershler equivalent circuit was first assumed [19]. In the Randles–Ershler equivalent circuit, any additional impedance associated with the non-uniform of electric field at the electrode/electrolyte interface and the variety of relaxation times is ignored [20–23]. Hence, the double layer capacity (C_d) is replaced by the parallel combination of C_d and b/ω, and this circuit was modified to be the parallel combination of the double layer capacity (C_d), b/ω and R_{ct} based on the Randles–Ershler equivalent circuit, as shown in Fig. 11, to take into consideration both the non-uniform of electric field at the electrode/electrolyte interface owing to the roughness of electrode surface, and the variety of relaxation times with adsorbed species on the electrode surface, although the physical meanings of θ and b have not been completely clarified. According to Fig. 11, we can obtain the total impedance $\mathbf{Z}$ as following:

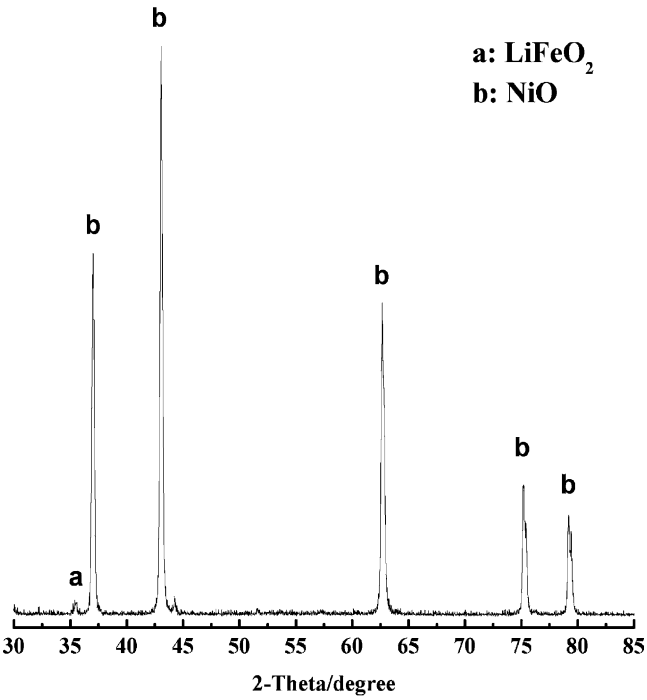

Fig. 7. X-ray diffraction patterns of $LiFeO_2$ coated porous NiO cathode sintered at 850 °C.

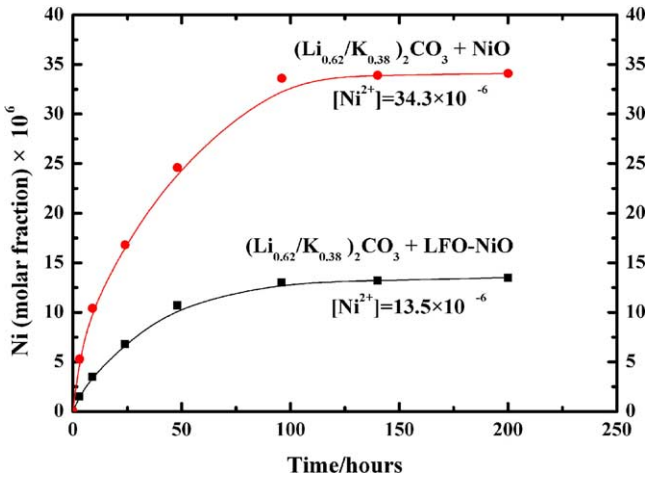

Fig. 8. Equilibrium solubility of nickel ions in the $(Li_{0.62}K_{0.38})_2CO_3$ melts shown as a function of immersion time ($T = 650$ °C, $P(CO_2) = 0.67$ atm, $P(O_2) = 0.33$ atm).

$$\mathbf{Z} = \frac{R_\Omega + 1}{j\omega C_d + \omega/b + 1/R_{ct}} \tag{1}$$

one obtains:

$$\mathbf{Z}_0 = \frac{1}{j\omega C_d + \omega/b + 1/R_{ct}} = \frac{bR_{ct}(b + \omega R_{ct})}{(b + \omega R_{ct})^2 + (\omega b C_d R_{ct})^2} - \frac{j\omega b^2 R_{ct}^2 C_d}{(b + \omega R_{ct})^2 + (\omega b C_d R_{ct})^2} = \mathbf{Z}' - j\mathbf{Z}'' \tag{2}$$

The ohmic and capacitive components of $\mathbf{Z}_0$ are $\mathbf{Z}'$ and $\mathbf{Z}''$ and result in:

$$\mathbf{Z}' = \frac{bR_{ct}(b + \omega R_{ct})}{(b + \omega R_{ct})^2 + (\omega b C_d R_{ct})^2} \tag{3}$$

$$\mathbf{Z}'' = \frac{\omega b^2 R_{ct}^2 C_d}{(b + \omega R_{ct})^2 + (\omega b C_d R_{ct})^2} \tag{4}$$

$$\frac{\mathbf{Z}'}{\mathbf{Z}''} = \frac{b + \omega R_{ct}}{\omega b C_d R_{ct}} = \frac{1}{bC_d} + \frac{1}{\omega C_d R_{ct}} \tag{5}$$

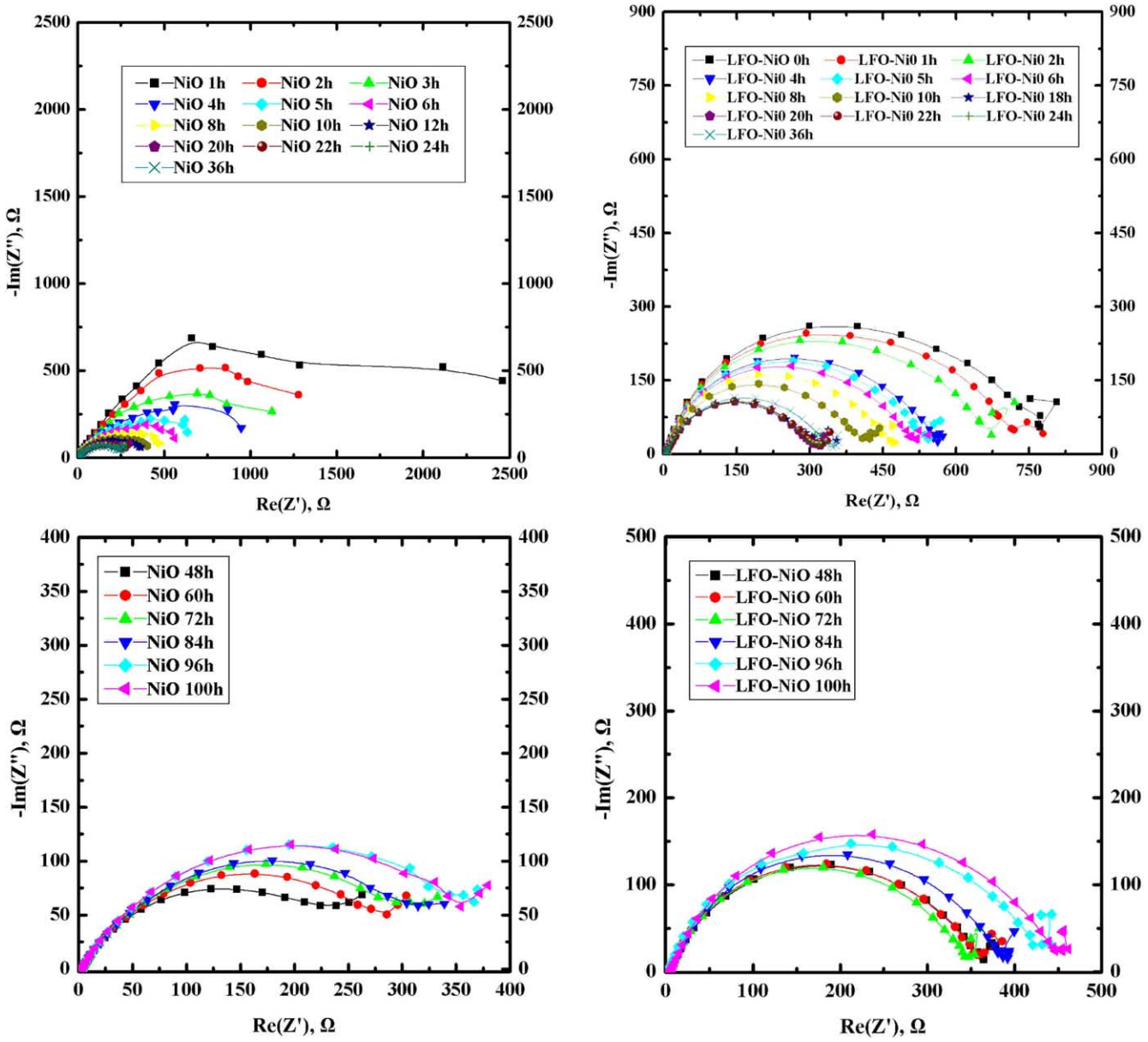

Fig. 9. Nyquist impedance spectra obtained for two cathode materials in the frequency range of 10 mHz to 100 kHz as a function of immersion time at 650 °C in standard cathode gas atmosphere (CO_2:O_2, 67:33%).

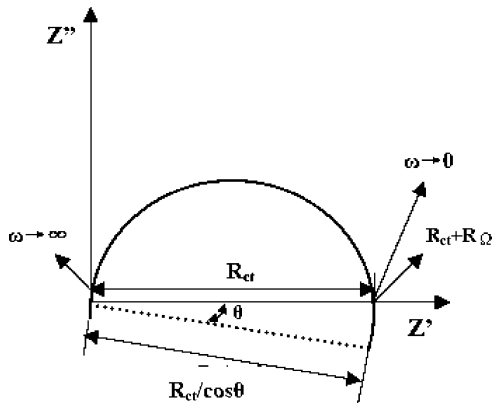

Fig. 10. Sketch map of rotation of semicircle on the complex plane.

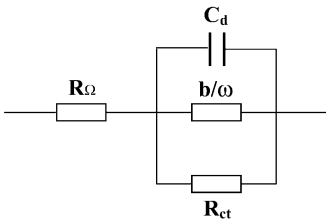

Fig. 11. Equivalent circuit corresponding to rotation of semicircle on the complex plane based on the generalized Randles–Ershler equivalent circuit model.

$$\frac{1}{\omega C_d R_{ct}} = \frac{Z'}{Z''} - \frac{1}{bC_d} \quad (6)$$

it follows from Eq. (7):

$$Z'' = \frac{R_{ct}}{\omega C_d R_{ct}[(b+\omega R_{ct})^2/(\omega b C_d R_{ct})^2 + 1]} \quad (7)$$

$$Z'' = \frac{R_{ct}[Z'/Z'' - 1/(bC_d)]}{(Z'/Z'')^2 + 1} = \frac{Z'' R_{ct}[Z' - Z''/(bC_d)]}{Z'^2 + Z''^2} \quad (8)$$

$$Z'^2 + Z''^2 = R_{ct}Z' - Z'' R_{ct}/bC_d \quad (9)$$

namely,

$$\left(\frac{Z' - R_{ct}}{2}\right)^2 + \frac{Z'' + R_{ct}}{(2bC_d)^2} = \frac{R_{ct}^2}{4 + 4/(bC_d)^2} \quad (10)$$

according to Eq. (7):

$$\frac{dZ''(\omega)}{d\omega} = \frac{b^2 R_{ct}^2 C_d (b^2 - \omega^2 b^2 R_{ct}^2 C_d^2 - \omega^2 R_{ct}^2)}{[(b+\omega R_{ct})^2 + (\omega b C_d R_{ct})^2]^2} \quad (11)$$

with the relation:

$$\frac{dZ''}{d\omega} = 0 \, (\omega = \omega^*) \quad (12)$$

we can find:

$$\omega^{*2} R_{ct}^2 (1 + b^2 C_d^2) = b^2 \quad (13)$$

if we appoint:

$$tg\theta = \frac{1}{bC_d} \quad (14)$$

then,

$$b = \frac{\omega^* R_{ct}}{\sin\theta} \quad (15)$$

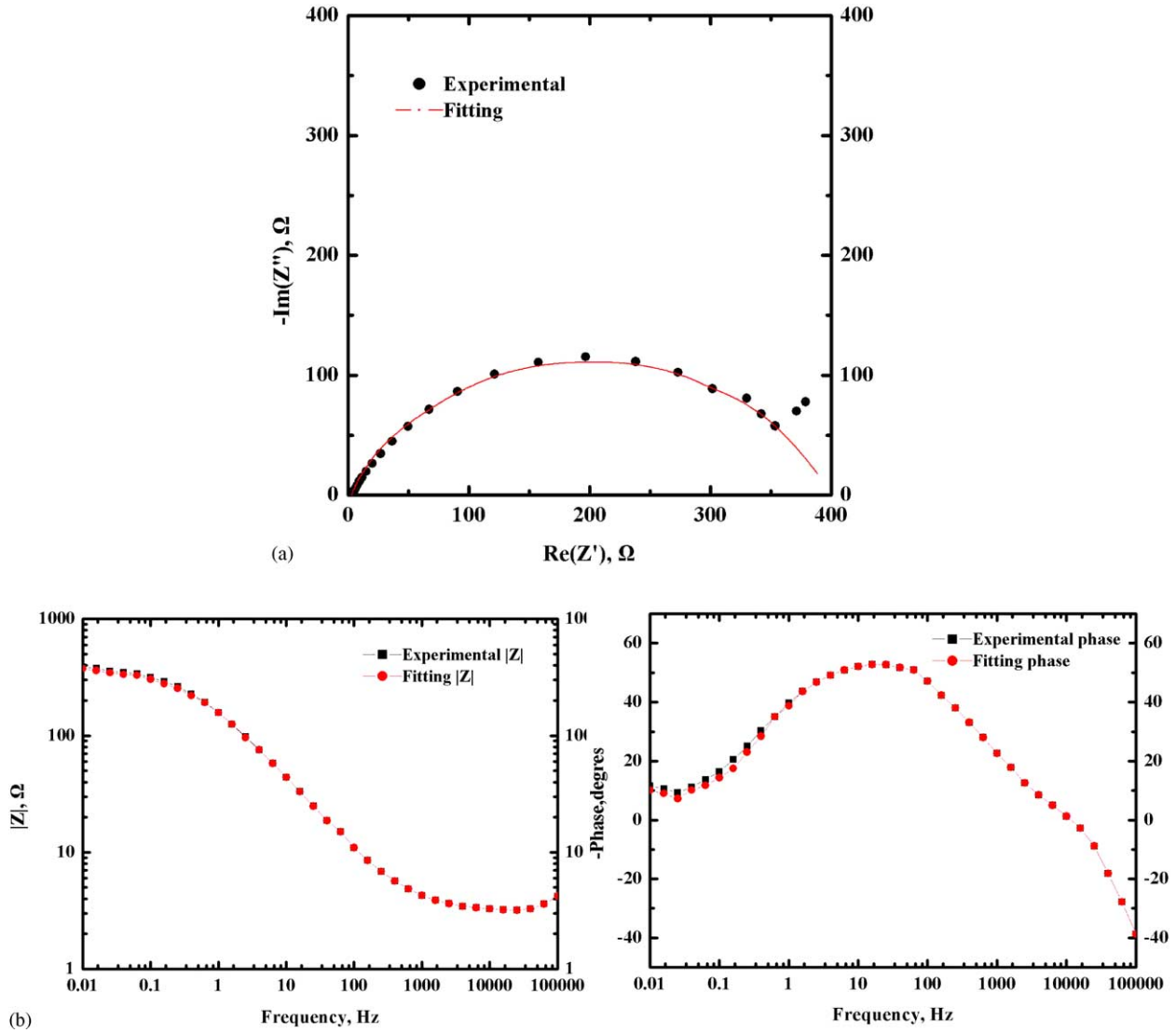

Fig. 12. Measured impedance spectra for NiO cathode in the frequency range of 10 mHz to 100 kHz at 100 h at 650 °C in standard cathode gas atmosphere (CO_2:O_2, 67:33%) compared to spectra calculated following Eq. (1): (a) Nyquist plot; (b) Bode plot.

$$C_d = \frac{\cos\theta}{\omega^* R_{ct}} \quad (16)$$

where b is a constant, ω the angular frequency, ω^* the angular frequency corresponding to the apex of semicircular arc.

Here, it is noted that the real charge transfer resistance, R_{ct}, is not equal to the diameter of rotated semicircle, but to the length of chord overlapping on the real axis. Therefore, the charge transfer resistance (R_{ct}) is equal to:

$$R_{ct} = (\text{the diameter of rotated semicircle}) \cos\theta \quad (17)$$

All impedance spectra were fitted to Eq. (1) which corresponded to the modified Randles–Ershler equivalent circuit that considered both the non-uniform of electric field at the electrode/electrolyte interface owing to the roughness of electrode surface, and the variety of relaxation times with adsorbed species on the electrode surface. In all cases, the fits were very satisfactory in the whole frequency range. The NiO and LFO-NiO cathode samples can be seen in Figs. 12 and 13, where the experimental and fitted data are depicted in the Nyquist and Bode diagrams for two cathode samples at 100 h of immersion. All experimental plots could be well described theoretically with the modified Randles–Ershler equivalent circuit model. Tables 2 and 3 summarized the fitting values of parameters for oxygen reduction reaction on oxide electrodes in Li/K eutectic melts under a 0.67 atm CO_2/0.33 atm O_2 atmosphere at different immersion time.

As can be seen from Fig. 9 and Tables 2 and 3, the electrolytic resistance is almost independent of immersion time. The diameter of semicircular arc (denotes the charge transfer resistance R_{ct}) is decreasing sharply with time initially. This implies that, in the case of two cathode materials, the electrochemical reaction rates are increasing rapidly with time. The reason could be the incorporation of lithium in their structure, which enhances their electronic conductivity. Then, the semicircular arc increases gradually with time

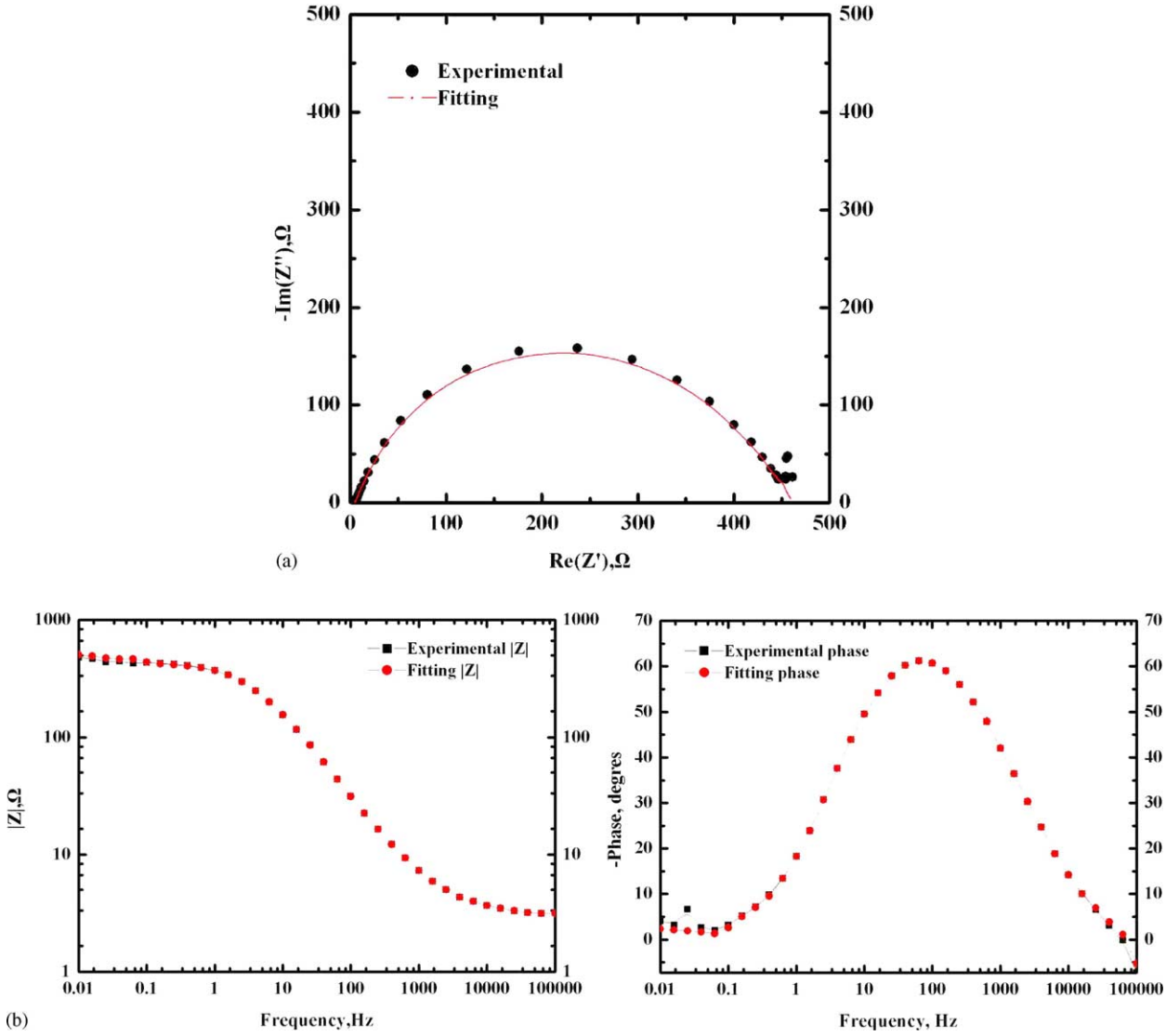

Fig. 13. Measured impedance spectra for LFO-NiO cathode in the frequency range of 10 mHz to 100 kHz at 100 h at 650 °C in standard cathode gas atmosphere (CO_2:O_2, 67:33%) compared to spectra calculated following Eq. (1): (a) Nyquist plot; (b) Bode plot.

Table 2
Fitting results for oxygen reduction on NiO electrode in Li/K eutectic melts at different immersion time

Time (h)	R Ω/Ω	R_{ct} (Ω)	C_d (μF)	θ (°)	b (Ω)
2	2.1485	1791.00	2288	28.289	812.087
4	2.2398	999.26	2831.40	33.894	525.709
6	2.3018	633.49	1777.40	33.453	851.542
8	2.2036	531.85	1726.20	34.299	849.264
10	2.3925	419.19	1241.80	35.009	1149.678
12	2.6951	342.69	987.94	32.590	1583.353
20	2.8493	292.67	1056.70	33.704	1418.766
22	2.3876	279.40	1031.70	35.376	1365.112
24	2.2413	291.55	1077.90	36.957	1233.063
36	2.3837	275.45	1022.20	36.679	1313.471
48	2.0634	298.26	902.56	36.991	1470.793
72	3.0407	338.28	1002.50	30.400	1700.208
96	3.1092	397.06	941.65	29.693	1862.353
100	3.2255	392.51	912.94	29.129	1965.636

Atmosphere: 0.67 atm CO_2/0.33 atm O_2; $T = 650\,^{\circ}C$.

suggesting that the corresponding electrochemical reaction rates are decreasing slowly with time (in terms of NiO, LFO-NiO, after 22 and 24 h, respectively). The reason could be the slow dissolution of two cathode materials in molten carbonates. According to Tables 2 and 3, we can find that the semicircular arc of LFO-NiO cathode is a little larger than that of the pure NiO cathode at 72–100 h of immersion in molten carbonate in the high frequency region. This suggests that $LiFeO_2$ coating has a slightly negative influence in the charge transfer processes associated with the oxygen reduction reaction. However, the LFO-NiO cathode shows a low charge transfer resistance close to the NiO value. Taking into consideration the crack of NiO cathode in the eutectic Li/K carbonate melts, more work is required to confirm the long-term electrochemical characterization of the LFO-NiO cathode.

In addition, we have compared the efficiency of a cell using a NiO cathode with that using a $LiFeO_2$ coated NiO cathode, tests were performed on an 9.5 cm × 9.5 cm unit cell at 650 °C. An Ni–10 wt.% Cr electrode was used as the anode, porous γ-$LiAlO_2$ plate was used as the matrix, and $(Li_{0.62}K_{0.38})_2CO_3$ plate was used as the electrolyte. The anode gas composition was 64% H_2–16% CO_2–20% H_2O and the cathode gas composition was 70% air–30% CO_2.The cells with the conventional NiO cathode and the LFO-NiO cathode were tested for about 300 and 510 h of heating time (time after electrolyte melting), respectively. The polarization curves of the operations are shown in Fig. 14. In the case of the NiO cathode (Fig. 14a), we can observe a continuous decrease of the performance with time, especially at a high electronic load. However, the polarization curves for the LFO-NiO cathode (Fig.14b) maintains more stable values. The high performance of the cell seems to be due to $LiFeO_2$ coating on the NiO surface. In other words, due to its excellent stability in carbonate melts under the standard conditions, the $LiFeO_2$ coating significantly retards the dissolution of the inner NiO in the eutectic Li/K carbonate melts. It can be inferred that the coating of $LiFeO_2$ on the surface of the NiO cathode is a good alternative cathode manufacturing method for MCFC.

Table 3
Fitting results for oxygen reduction on $LiFeO_2$ coated NiO electrode in Li/K eutectic melts at different immersion time

Time (h)	R Ω/Ω	R_{ct} (Ω)	C_d (μF)	θ (°)	b (Ω)
0	4.1588	725.65	73.248	16.726	45,430.408
2	3.2745	665.67	77.253	18.193	39,387.080
4	3.2610	559.51	73.654	18.260	41,149.384
6	3.6523	507.15	72.226	18.700	40,904.560
8	4.1033	449.54	69.963	17.692	44,808.331
10	3.9884	400.87	64.153	18.846	45,668.455
18	4.7947	303.94	54.582	19.429	51,941.537
20	4.6213	302.38	54.928	19.258	52,109.601
22	4.6177	301.32	56.564	19.203	50,758.871
24	4.6186	297.54	55.397	19.403	51,251.501
36	3.9700	334.38	59.383	19.970	46,342.555
48	3.7387	358.28	61.665	20.085	44,350.065
72	3.3878	344.62	65.617	20.108	41,627.118
96	3.4451	412.32	69.422	19.480	40,722.662
100	3.5019	424.65	69.499	19.463	40,715.966

Atmosphere: 0.67 atm CO_2/0.33 atm O_2; $T = 650\,^{\circ}C$.

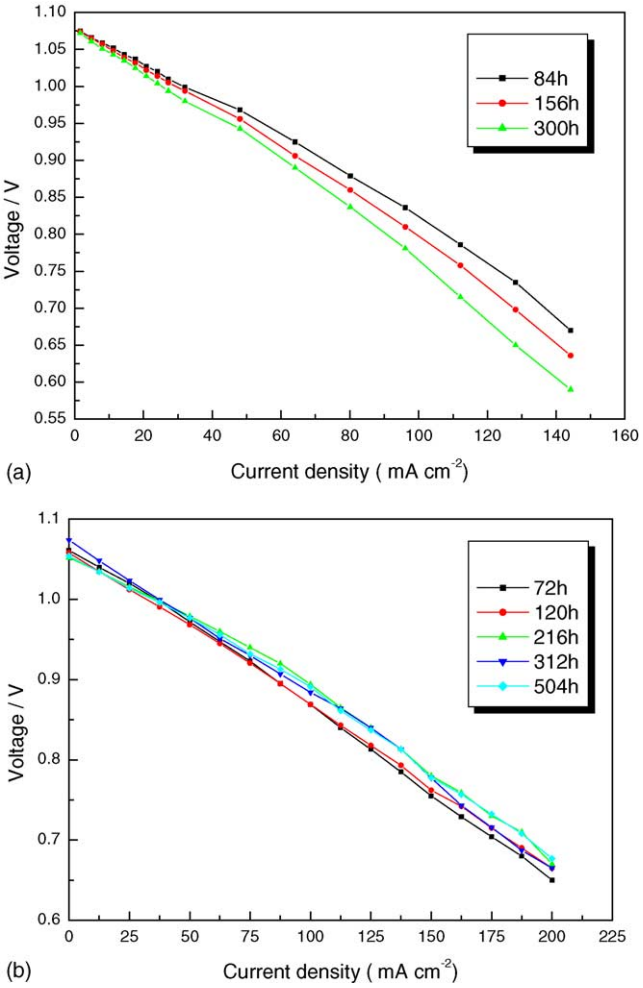

Fig. 14. Voltage–current density curves for both cathodes: (a) NiO cathode; (b) LFO-NiO cathode.

4. Conclusions

$LiFeO_2$ was coated on the state-of-the-art porous NiO cathode using a simple combustion process. $LiFeO_2$ coating followed by sintering yielded electrodes with good pore structure. No significant differences in the particle size and the surface morphology of $LiFeO_2$ coated NiO cathode were observed before and after immersion in the eutectic molten Li/K carbonates for 200 h.

The short-term stability tests in the eutectic molten Li/K carbonates at 650 °C showed that the coating of $LiFeO_2$ on NiO was dramatically effective in reducing nickel dissolution. The electrochemical behavior of the NiO and LFO-NiO cathodes in the eutectic molten Li/K carbonates at 650 °C was also investigated by EIS as a function of immersion time in the presence of the standard cathode gas condition. The impedance response of the NiO and LFO-NiO at different immersion time was characterized by the presence of depressed semicircles in the high frequency range changing over into the lines with the angle of which observed with the real axis differing 45° or 90° in the low frequency range. The experimental Nyquist plots could be well analyzed theoretically with a modified model based on the well known Randles–Ershler equivalent circuit model. In the new model, this circuit was modified to be the parallel combination of the double layer capacity (C_d), b/ω and the charge transfer resistance (R_{ct}), to take into consideration both the non-uniform of electric field at the electrode/electrolyte interface owing to the roughness of electrode surface, and the variety of relaxation times with adsorbed species on the electrode surface. The cathode that was prepared with coating method to coat $LiFeO_2$ on the surface of NiO cathode was able to reduce the solubility of NiO to lengthen the lifetime of MCFC while maintaining the advantages of NiO cathode. Therefore, it could be used as an alternative cathode for MCFC. We made novel alternative cathode material using coating of $LiFeO_2$ on the surface of the NiO cathode. Using the manufacturing method, we expect that economical and large-scale cathode can be made easily.

Acknowledgements

The authors thank the Shanghai Committee of Science and Technology and the Postdoctoral Foundation of China (Grant No. 2003003295) for the grants that support this research.

References

[1] Y. Ito, K. Tsuru, J. Oishi, Y. Miyazaki, K. Teruo, J. Power Sources 23 (4) (1988) 357–364.
[2] P. Ganesan, H. Colon, B. Haran, R. White, B.N. Popov, J. Power Sources 111 (2002) 109–120.
[3] A. Durairajan, H. Colon-Mercado, B. Haran, R. White, B. Popov, J. Power Sources 104 (2002) 157–168.
[4] T. Nishina, I. Uchida, Optimization of cathode gas compositions for MCFC using simplified thin film model, Denki Kagaku Oyobi Kogyo Butsuri 64 (6) (1996) 513–518.
[5] K. Yong, H. Selman, J. Robert, Mechanism of low-CO_2 performance of the MCFC cathode, Proc. Electrochem. Soc. 94 (13) (1994) 781–787.
[6] J.R. Selman, M.S. Alicia, Y. Lzaki, Nickel oxide cathode dissolution in the MCFC: a review, Prepr. Pap.-Am. Chem. Soc., Div. Fuel Chem. 38 (4) (1993) 1429–1434.
[7] W.H.A. Peelen, M. Van Driel, K. Hemmes, J.H.W. De Wit, Electrochim. Acta 43 (21–22) (1998) 3313–3331.
[8] J.L. Smith, G.H. Kucera, A.P. Brown, in: Molten Carbonate Fuel Cell Technology, PV90-16, Electrochem. Soc. Softbound Proc. Ser., Pennington, NJ, 1990, p. 226.
[9] S.T. Kuk, Y.S. Song, K. Song, J. Power Sources 83 (1999) 50–56.
[10] P. Ganesan, H. Colon, B. Haran, B.N. Popov, J. Power Sources 115 (2003) 12–18.
[11] F. Li, H.-Y. Chen, C.-M. Wang, K.-A. Hu, J. Electroanal. Chem. 531 (1) (2002) 53–60.
[12] F. Li, C.-M. Wang, K.-A. Hu, Mater. Res. Bull. 37 (2002) 1907–1921.
[13] S. Jain, K. Adiga, V. Vrneker, Combust. Flame 40 (1981) 71.
[14] L. Giorgi, M. Carewska, M. Patriarca, S. Scaccia, E. Simonetti, A. Di Bartolomeo, J. Power Sources 49 (1994) 227–243.
[15] F.J. Perez, D. Duday, M.P. Hierro, J.A. Alonso, M.J. Martýnez, L. Daza, J. Power Sources 86 (2000) 309–315.
[16] A.J. Appleby, S.B. Nicholson, J. Electroanal. Chem. 53 (1974) 105.
[17] I. Uchida, T. Nishina, Y. Mugikura, K. Itaya, J. Electroanal. Chem. 206 (1986) 229–239.
[18] N. Motohira, T. Sensou, K. Yamauchi, K.O. Gawa, X. Liu, N. Kamiya, K. Ota, J. Mol. Liq. 83 (1999) 95–103.
[19] J.E.B. Randles, Disc. Faraday Soc. 1 (1947) 11;
D.C. Grahame, J. Electrochem. Soc. 99 (1952) C370.
[20] J.N. Sarmousakis, M.J. Prager, J. Electrochem. Soc. 104 (1957) 454.
[21] R. De Levie, Electrochim. Acta 10 (1965) 113.
[22] G.M. Schmid, Electrochim. Acta 15 (1970) 65.
[23] S. Iseki, K. Ohashi, S. Nagaura, Electrochim. Acta 17 (1972) 2249.